Journal of Zhejiang University-SCIENCE A (Applied Physics & Engineering)
ISSN 1673-565X (Print); ISSN 1862-1775 (Online)
www.jzus.zju.edu.cn; www.springerlink.com
E-mail: jzus@zju.edu.cn

Design of transition curve of profiled chamber flow sensor considering slides with arc ends*

Li LIU, Yang LU‡

School of Aeronautics and Astronautics, Zhejiang University, Hangzhou 310027, China

E-mail: liulizju@zju.edu.cn; zd_luyang@126.com

Received Oct. 8, 2016; Revision accepted May 11, 2017; Crosschecked Jan. 15, 2018

Abstract: The face-shaped curve of the stator inner chamber of the profiled chamber flow sensor is formed with two quarters of circular arcs and two quarters of noncircular arcs. The two quarters of noncircular arcs are normally defined as transition curves. The parameters of the transition curves directly affect the dynamic performance of the sensor system. Therefore, the design and optimization of the transition curves is a most important part in the design of the system. Based on our previous work, this paper discusses more general expressions of the boundary conditions and derivations of the transition curves. The optimization of the transition curves considering slides with arc ends as the most concentrated part is presented in detail. Firstly, the concept of "basic transition curve" is proposed. Secondly, the boundary conditions and derivations of the basic transition curves are discussed and general expressions using a polynomial function are given. Then, the concave-convex direction of the basic transition curve is analyzed. Lastly, the transition curves considering the slides with arc ends are analyzed when the arc ends have equivalent radius with the major radius of the stator.

Key words: Profiled chamber flow sensor; Transition curve; Optimal design; Curve curvature
https://doi.org/10.1631/jzus.A1600666 **CLC number:** TH113

1 Introduction

As a new type of rotary positive-displacement flow sensor, the profiled chamber flow (PCF) sensor consists mainly of a stator with an inner profiled chamber and a rotor-slides assembly as described in our previous work (Lu, 2007; Wu et al., 2009; Lei et al., 2010). Fig. 1 shows the basic configuration of a bidirectional PCF. The stator of the bidirectional PCF is a hollow noncircular cylinder with an inner profiled chamber and other functional structures including an inlet port, an outlet port, and two diversion grooves. The inner chamber profile is symmetric and consists of (i) fixed curves: two circular arcs $\overset{\frown}{AB}$ with radius R and $\overset{\frown}{CD}$ with radius r ($R>r$), and (ii) transition curves: two noncircular arcs $\overset{\frown}{BC}$ and $\overset{\frown}{AD}$, each with the same shape and size. Arcs $\overset{\frown}{AB}$ and $\overset{\frown}{CD}$ are coaxial, while the transition curves $\overset{\frown}{BC}$ and $\overset{\frown}{AD}$ are symmetrical, and have their major radii equal to R and minor radii equal to r. The shape of the transition curves affects the impact, penetration, friction, and wear of the slides-chamber assembly. Therefore, the design of the transition curves of $\overset{\frown}{BC}$ and/or $\overset{\frown}{AD}$ is of great interest, and this logically comes down to simultaneously satisfying particular requirements in kinematics and geometry. This process is similar to normal optimizations of cam mechanisms (Mandal and Naskar, 2009; Flocker, 2012). The design of transition curves can be also applied in many other areas such as highway and railway route design (Cai and Wang, 2009). One objective of the transition curve design is to optimize the values of acceleration and jerk of the slides. That is, the slide motion

‡ Corresponding author
* Project supported by the Zhejiang Provincial Natural Science Foundation of China (No. Z1110190)
ORCID: Li LIU, https://orcid.org/0000-0001-8986-8073

function must be continuous through the first (velocity) and second (acceleration) derivatives across the entire cycle, and the motion function must be finite or continuous through the third (jerk) derivative across the entire interval (Naskar and Mishra, 2012). Some other limitations are adopted due to specific usage (Cardona et al., 2002).

Polynomial functions with different orders are widely employed in cam transition curve design (Yu and Lee, 1998; Mermelstein and Acar, 2004; Acharyya and Naskar, 2008) and are also adopted in the optimization of transition curves of the PCF sensor (Lei and Lu, 2011). Lei and Lu (2011) analyzed the geometric features and requirements of the kinematics and deduced the goal functions in polynomial forms with the 3rd, 5th, 7th, and 9th orders for the transition curves. They discussed the dynamic properties including velocity, acceleration, and jerk of their derived functions and concluded that the 5th-order polynomial transition curve has optimal synthesized performance among the 3rd-, 5th-, 7th-, and 9th-order polynomial transition curves.

The present work is based on our work described above and is to give general expressions of the boundary conditions and derivations of the transition curves of the bidirectional PCF. The curvature of the transition curves is also considered. Further, the present work examines the design of transition curves of the slides with arc ends.

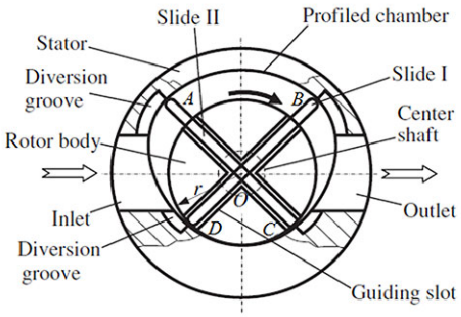

Fig. 1 Configuration of the bidirectional profiled chamber flow sensor

2 Basic transition curve and its curvature

The working mechanics of PCF require that the transition curve $\overset{\frown}{BC}$ must be changed continuously and smoothly from point B to point C (Lei and Lu, 2011) (Fig. 2).

When a slide is at the initial position (Fig. 3), we let $OB_s=r_1$, $OD_s=r_2$, $r_2<r_1$. B_s and D_s are the right and left end points of the slide, respectively. As the slide rotates, the radial distance from the chamber center O to B_s, defined as ρ_s, is a function of the rotation angle θ, which is determined with the x-axis as its starting line. Lei and Lu (2011) considered the slides as straight lines, neglecting the thickness of the slide, so that the point-contact between the slides and the chamber occurs at the pointed ends (B_s and D_s) of the slides. In this case, $r_1=R$ and $r_2=r$. In the present analysis, we also suppose $\rho_s(\theta)$ is a polynomial function of the following form, k_i (i=1, 2, …, n) is the coefficient of the polynomial function, and $\rho_s(\theta)$ is called the "basic transition curve".

$$\rho_s(\theta)=r_1+(r_1-r_2)\left[k_{(n+1)/2}\bar{\theta}^{(n+1)/2}+k_{(n+1)/2+1}\bar{\theta}^{(n+1)/2+1}+\ldots+k_n\bar{\theta}^n\right], \quad (1)$$

$$\bar{\theta}=\theta/(\pi/2).$$

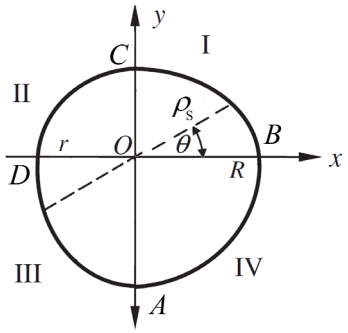

Fig. 2 Face-shaped curve of the inner profiled chamber of the bidirectional PCF

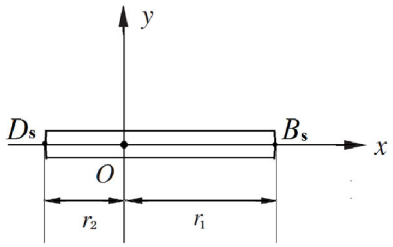

Fig. 3 A slide of the bidirectional PCF at the initial position

Compared with our previous work (Lei and Lu, 2011), general expressions and analysis of the basic transition curve $\rho_s(\theta)$ are derived in the present study based on proper boundary conditions, see Appendix

A. It also demonstrates that the order of $\rho_s(\theta)$, n, should be odd and $n\geq 5$.

The solutions of the coefficients of the 5th-, 7th-, 9th-, and 11th-order polynomial functions are given as follows:

$$\begin{aligned}
&\boldsymbol{k}(n=5)=[k_3,k_4,k_5]^{\mathrm{T}}=[-10,15,-6]^{\mathrm{T}},\\
&\boldsymbol{k}(n=7)=[k_4,k_5,k_6,k_7]^{\mathrm{T}}=[-35,84,-70,20]^{\mathrm{T}},\\
&\boldsymbol{k}(n=9)=[k_5,k_6,k_7,k_8,k_9]^{\mathrm{T}}\\
&\qquad=[-126,420,-540,315,-70]^{\mathrm{T}},\\
&\boldsymbol{k}(n=11)=[k_6,k_7,k_8,k_9,k_{10},k_{11}]^{\mathrm{T}}\\
&\qquad=[-462,1980,-3465,3080,-1386,252]^{\mathrm{T}}.
\end{aligned}$$

The kinematic characteristics of the basic transition curve can be described by the change rate (v) of the polar radius ρ_s with time T:

$$v=\frac{\mathrm{d}\rho_s}{\mathrm{d}T}=\omega\frac{\mathrm{d}\rho_s}{\mathrm{d}\theta}=\omega\rho_s',\quad a=\omega^2\rho_s'',\quad j=\omega^3\rho_s''',$$

where ω is the angular velocity of the slide and is assumed to be constant. a and j are the 1st- and 2nd-order derivatives of ρ_s with time, respectively. Then we can define: $V=\rho_s'$, $A=\rho_s''$, and $J=\rho_s'''$ as the velocity, acceleration, and jerk of the basic transition curve, where ρ_s' denotes $\mathrm{d}\rho_s/\mathrm{d}\theta$, ρ_s'' denotes $\mathrm{d}^2\rho_s/\mathrm{d}\theta^2$, and ρ_s''' denotes $\mathrm{d}^3\rho_s/\mathrm{d}\theta^3$. Fig. 4 shows the changes of velocity, acceleration, and jerk with normalized polar angle $\bar{\theta}$ for different values of n. It is clear that when $n\geq 7$, the V, A, and J curves of the transition curves are all continuous and smooth across the entire interval for $0\leq\bar{\theta}\leq 1$. The maximum values of V, A, and J of the basic transition curve of n=7 are minimal among the curves of n=7, 9, 11, …. When n=5, the J curve of the basic transition curve is not continuous at $\bar{\theta}$=0 and $\bar{\theta}$=1. However, the maximum values of V and A of the basic transition curve of n=5 are minimal among the curves of n=5, 7, 9, 11, …. Therefore, the basic transition curve of n=5 is the best at "V-criterion" and n=7 is the best at "J-criterion" (Lei and Lu, 2011). This analyzing method is called "V-A-J method" (Lei et al., 2016).

Since the 5th- and 7th-order polynomial functions could be optimal for transition curves, in the following analysis, the 5th-order polynomial function is taken as an example. The basic transition curve is expressed as

$$\begin{aligned}
&\rho_s(\theta)=r_1+(r_1-r_2)\left(-10\bar{\theta}^3+15\bar{\theta}^4-6\bar{\theta}^5\right),\\
&\bar{\theta}=\theta/(\pi/2).
\end{aligned}\tag{2}$$

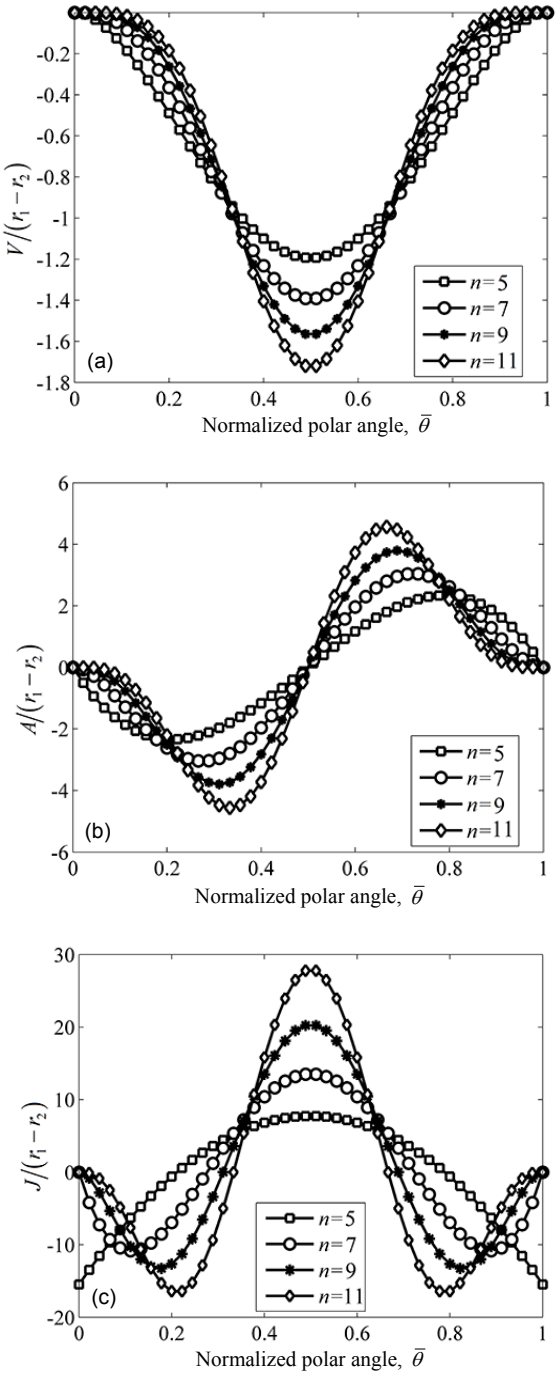

Fig 4 Changes of V (a), A (b), and J (c) with normalized polar angle for different basic transition curves

A 5th-order polynomial function of $\rho_s(\theta)$ with different values of the ratio, r_2/r_1, is analyzed and it is found that the value of r_2/r_1, which is in the range of (0, 1), affects the curve shape, or the curvature, of the basic transition curve, as shown in Fig. 5. When the value of r_2/r_1 is as large as 0.8, the basic transition curve is concave throughout the whole interval; when it is as small as 0.5, the basic transition curve turns from concave to convex and then to concave again. Due to some practical design considerations, like avoiding surface interference and inappropriate tool cutting (Nguyen and Kim, 2007; Wu et al., 2007; Fujiki et al., 2011) or obtaining proper contact stresses and deformations of the slides and the chamber at the point of contact (Carra et al., 2004; Hidalgo-Martínez et al., 2014), it is necessary to analyze the curvatures of the transition curves of the chamber as it is in the design of cam-follower system (Wu et al., 1999; Yan and Cheng, 1999; Chablat and Angeles, 2007).

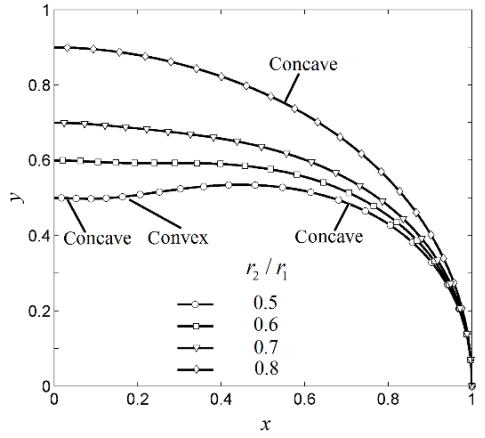

Fig. 5 Shapes of the transition curves of the 5th-order polynomial function with different values of r_2/r_1

The curvature (κ) of a curve $y=y(x)$ can be expressed as

$$\kappa=\frac{y''(x)}{\left[1+y'^2(x)\right]^{\frac{3}{2}}}. \tag{3}$$

For the basic transition curve in the first quadrant,

$$\begin{aligned} x&=\rho_s(\theta)\cos(\theta),\\ y&=\rho_s(\theta)\sin(\theta). \end{aligned} \tag{4}$$

Then the curvature of the basic transition curve can be expressed as

$$\begin{aligned}\kappa&=\frac{\mathrm{d}\left(\frac{\mathrm{d}y}{\mathrm{d}\theta}\Big/\frac{\mathrm{d}x}{\mathrm{d}\theta}\right)\Big/\mathrm{d}\theta}{\mathrm{d}x/\mathrm{d}\theta}\Bigg/\left[1+\left(\frac{\mathrm{d}y}{\mathrm{d}\theta}\Big/\frac{\mathrm{d}x}{\mathrm{d}\theta}\right)^2\right]^{3/2}\\ &=\frac{\rho_s''\rho_s-2\rho_s'^2-\rho_s^2}{\left(\rho_s'^2+\rho_s^2\right)^{3/2}}.\end{aligned} \tag{5}$$

The radius of curvature is

$$\rho_\kappa=1/\kappa=\frac{\left(\rho_s'^2+\rho_s^2\right)^{3/2}}{2\rho_s'^2-\rho_s''\rho_s+\rho_s^2}. \tag{6}$$

The curvature κ and the radius of curvature ρ_κ can be positive or negative, which depends on the concave-convex direction of the designed basic transition curve of $\rho_s(\theta)$. With different values of r_2/r_1, Fig. 6 shows curvature κ as a function of $\bar{\theta}$ in the first quadrant with r_1=1.

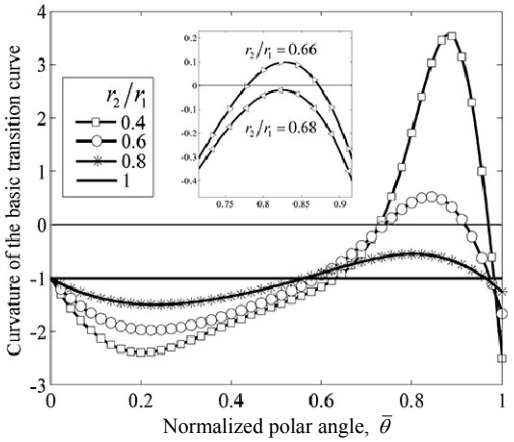

Fig. 6 Curvature κ as a function of normalized polar angle $\bar{\theta}$ and size ratio r_2/r_1 for the 5th-order polynomial function

In order for the inner face-shape of the chamber to have best manufacturability, including processing and dimensions measurement of the chamber, the transition curve should be concave throughout the whole interval. If the value of κ is negative through 0 to 1 of angle $\bar{\theta}$, the transition curve is concave. It can be seen from Fig. 6 that, for a 5th-order polynomial

function, if the value of r_2/r_1 is smaller than 0.66, the value of κ will become positive for a certain range of $\bar{\theta}$, and the curve turns from concave to convex and then to concave again. To obtain a more accurate value of r_2/r_1 and to keep the value of κ negative, we have tried a set of values of r_2/r_1 in the range of (0.66, 0.68) and found the turning value of r_2/r_1 is around 0.677, which means, as long as $r_2/r_1 \geq 0.677$, a 5th-order basic transition curve is concave and suitable for manufacturability. For the 7th-, 9th-, and 11th-order basic transition curves, the turning values of r_2/r_1 are 0.728, 0.771, and 0.804, respectively. The suitable design ranges of r_2/r_1 for the 5th-, 7th-, 9th-, and 11th-order basic transition curves are $0.677 \leq r_2/r_1 \leq 1$, $0.728 \leq r_2/r_1 \leq 1$, $0.771 \leq r_2/r_1 \leq 1$, and $0.804 \leq r_2/r_1 \leq 1$, respectively.

If the slides have pointed ends (Fig. 7), the point-contact between the slides and the chamber occurs at the pointed ends of the slides. In this case, the thickness of the slides can be neglected and the slides can be considered as straight lines. The transition curve can be designed exactly as the basic transition curve from Eq. (1) with $r_1=R$ and $r_2=r$. The curvature analysis above is also applicable here. Except in this special condition, the thickness of the slides and the shape of its ends need to be considered.

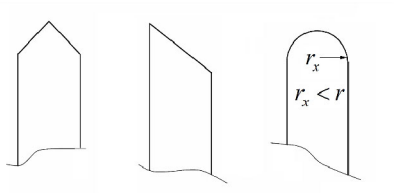

Fig. 7 Some sharp ends of the slides

3 Transition curves considering slides with arc ends

In the present work, the arc radius of the slide is chosen to be R to obtain a better sealing property between the slide ends and the curve $\widehat{AB}$. In this case, when the slide is at the initial position (Fig. 3), $OB_s=r_1=R$. The contact between the chamber and the left part of the slide OD_s is shown in Fig. 8 (the dashed line). O_s is the arc center of the left end of the slide. Then we have (Appendix B)

$$OD_s = r_2 = R - \left(R\cos\theta_1 - r\cos\theta_2\right) < r, \tag{7}$$

where $\theta_1=\arcsin(t/(2R))$, $\theta_2=\arcsin(t/(2r))$, and t is the thickness of the slides.

Since the slide can be considered as a rigid body, the dynamic properties are determined by the motion of the center of mass, which is one-to-one correspondent to the motion of point B_s or D_s. Therefore, the trajectory of point B_s in the first quadrant or point D_s in the third quadrant is first considered by following the design of the basic transition curves with the *V-A-J* method, as discussed in Section 2.

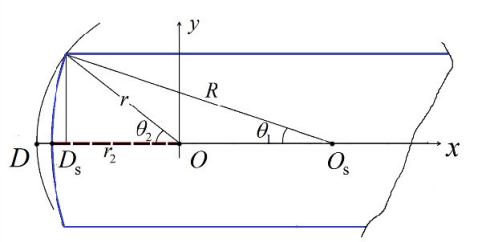

Fig. 8 Contact of the slide with the inner chamber

The trajectory curve of B_s is the basic transition curve with $r_1=R$ and in this case, a 5th-order basic transition curve is shown as

$$\begin{aligned}\rho_s(\theta) &= R + (R - r_2) \\ &\quad \times\left[-10\bar{\theta}^3 + 15\bar{\theta}^4 - 6\bar{\theta}^5\right], \\ 0 &\leq \bar{\theta} \leq 1.\end{aligned} \tag{8}$$

As shown in Fig. 9, the angle between OB_{1s} (or OB_{2s}) and OB_s is in Eq. (9) (see Appendix B):

$$\alpha(\theta) = \arctan\frac{t/2}{\rho_s(\theta) - R(1-\cos\theta_1)}. \tag{9}$$

It can be proved that α is a monotonically increasing function of θ when $0 \leq \theta \leq \pi/2$. The range of α is

$$0 < \alpha < \pi/4. \tag{10}$$

Then the trajectory curve of point B_{1s} is

$$\rho_{1s}(\beta_1) = \begin{cases} R, & 0 \leq \beta_1 \leq \alpha_1,\ \alpha_1 = \alpha(\theta = 0), \\ \dfrac{t/2}{\sin\alpha}, & \beta_1 = \theta + \alpha,\ 0 \leq \theta \leq \pi/2, \end{cases} \tag{11}$$

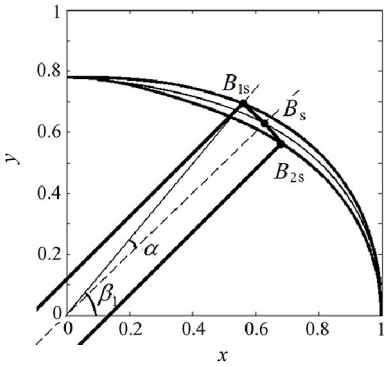

Fig. 9 Trajectory curves of the three representative points of the arc ends: B_s, B_{1s}, and B_{2s}

where $\alpha_1=\alpha(\theta=0)$, and β_1 is the rotation angle of OB_{1s}, determined with the x-axis as its starting line. The trajectory curve in Eq. (11) can also be expressed in Cartesian coordinates as follows:

$$\begin{aligned}&x=R\cos\beta_1,\ \ y=R\sin\beta_1,\quad 0\le\beta_1\le\alpha_1,\\&\text{and}\\&x=\frac{t}{2\sin\alpha}\cos(\theta+\alpha),\\&y=\frac{t}{2\sin\alpha}\sin(\theta+\alpha),\\&0\le\theta\le\pi/2.\end{aligned}\tag{12}$$

The trajectory curve of point B_{2s} is

$$\rho_{2s}(\beta_2)=\begin{cases}\dfrac{t/2}{\sin\alpha}, & \beta_2=\theta-\alpha,\ 0\le\theta\le\pi/2,\\ r_2, & \pi/2-\alpha_2\le\beta_2\le\pi/2,\ \ \alpha_2=\alpha(\theta=\pi/2),\end{cases}\tag{13}$$

where β_2 is the rotation angle of OB_{2s} determined with the x-axis as its starting line. The trajectory curve expressed under Cartesian coordinates is as follows:

$$\begin{aligned}&x=\frac{t}{2\sin\alpha}\cos(\theta-\alpha),\\&y=\frac{t}{2\sin\alpha}\sin(\theta-\alpha),\\&0\le\theta\le\pi/2,\\&\text{and}\\&x=r_2\cos\beta_2,\ \ y=r_2\sin\beta_2,\\&\pi/2-\alpha_2\le\beta_2\le\pi/2.\end{aligned}\tag{14}$$

Fig. 9 shows the trajectory curves of points B_s, B_{1s}, and B_{2s} when the value of θ varies from 0 to $\pi/2$.

3.1 Design of the transition curve

It is indicated from Fig. 9 that the transition curve in the first quadrant would be the trajectory curve of point B_{1s}. This speculation stands as long as $|O_sB_x|\ge|O_sB_{1s}|=R$ for any value of θ in the range from 0 to $\pi/2$, in which O_s is the arc center of $\overset{\frown}{B_{1s}B_{2s}}$, and B_x is the point on the trajectory curve of B_{1s} in the range of

$$\theta-\alpha(\theta)\le x+\alpha(x)\le\theta+\alpha(\theta),\ \ x\le\theta,\tag{15}$$

where $x+\alpha(x)$ is the rotation angle of OB_x determined with the x-axis as its starting line (Fig. 10a). If $x+\alpha(x)\ge\alpha_1$, then $|O_sB_x|$ can be calculated by

$$\begin{aligned}|O_sB_x|^2=&\left[\frac{t}{2\sin\alpha}\cos(x+\alpha)+(R-\rho_s)\cos\theta\right]^2\\&+\left[\frac{t}{2\sin\alpha}\sin(x+\alpha)+(R-\rho_s)\sin\theta\right]^2\\=&\left(\frac{t}{2\sin\alpha}\right)^2+(R-\rho_s)^2\\&+\frac{t(R-r_2)}{2\sin\alpha}\cos(x+\alpha-\theta),\\&\alpha=\alpha(x).\end{aligned}\tag{16}$$

Substituting $x=\theta$ into Eq. (16) we can obtain

$$\begin{aligned}|O_sB_{1s}|^2=&\left(\frac{t}{2\sin\alpha}\right)^2+(R-\rho_s)^2\\&+\frac{t(R-r_2)}{2\sin\alpha}\cos\alpha,\\&\alpha=\alpha(\theta).\end{aligned}\tag{17}$$

It is easy to prove that $|O_sB_x|\ge|O_sB_{1s}|$ with Eqs. (10), (15), (16), and (17).

If $-\alpha_1\le x+\alpha(x)\le\alpha_1$, the designed trajectory curve is an arc with radius R (Fig. 10b), and B_x is the point on the trajectory curve in the range of

$$\begin{aligned}&\theta-\alpha(\theta)\le x+\alpha(x)\le\alpha_1,\ \ x\le\theta,\\&\theta\ge0,\ \ \theta-\alpha(\theta)\le\alpha_1.\end{aligned}\tag{18}$$

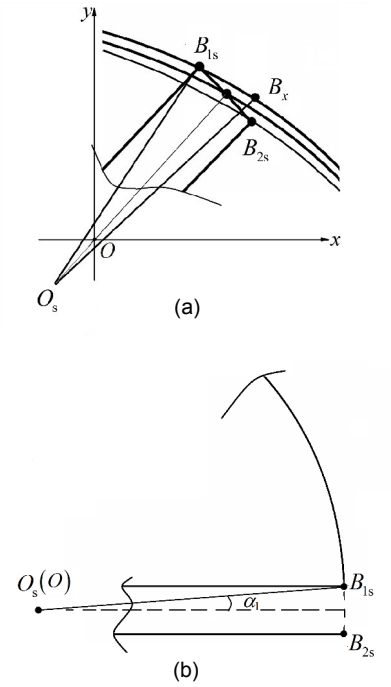

Fig. 10 Geometrical relationship between the slide and the three trajectory curves when the slide is at general position (a) and initial position (b)

In this case, $|O_sB_x|$ can be calculated by

$$\begin{aligned}|O_sB_x|^2 &= \left[R\cos(x+\alpha(x))+(R-\rho_s)\cos\theta\right]^2 \\ &\quad +\left[R\sin(x+\alpha(x))+(R-\rho_s)\sin\theta\right]^2 \\ &= R^2+(R-\rho_s)^2 \\ &\quad +2R(R-\rho_s)\cos(x+\alpha(x)-\theta).\end{aligned} \tag{19}$$

It is easy to prove that $|O_sB_x|\geq R$ with Eqs. (18) and (19).

It has been demonstrated that the transition curve should be the trajectory curve of point B_{1s} in the first quadrant and the trajectory curve of point B_{2s} in the third quadrant. Fig. 11 shows the whole profile of the rotor chamber with the designed transition curve of n=5. We should emphasize that the dynamic properties of the slides, the *V*-*A*-*J* curves, are the same as those shown in Fig. 4.

3.2 Curvature of the transition curve

In the first quadrant, the curvature of the transition curve can be derived from Eqs. (3), (5), and (12), but a direct derivation can lead to very long mathematical expressions that are cumbersome to work with. The curvature κ as a function of normalized polar angle with different values of r_2/r_1 can be calculated numerically with industrial mathematical software using Eqs. (3) and (12), as shown in Fig. 12 with R=1 and t/R=0.2. The turning value of r/R in this case is around 0.656, which means, as long as $r/R\geq$ 0.656, a 5th-order transition curve is concave throughout the first quadrant. It is also found that the turning value of r/R depends on both the order n and the value of t/R (Fig. 13).

As discussed in Section 2, the 5th- and 7th-order transition curves would be the best two designs for "*V*-criteria" and "*J*-criteria", respectively. In Fig. 13, the line with circles and the line with hexagons are the turning values of r/R for the 5th- and 7th-order transition curves, respectively, for different thicknesses of the slides. As long as the values of r/R are larger than the lines in Fig. 13, the transition curves are concave throughout the interval.

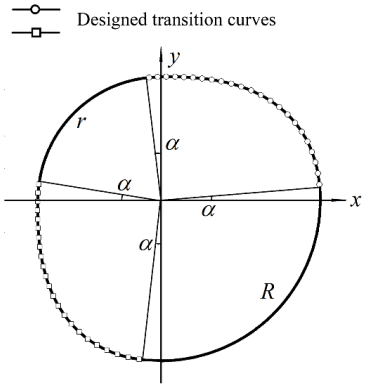

Fig. 11 Whole face-shaped curve of the inner chamber, r/R=0.77, t/R=0.2

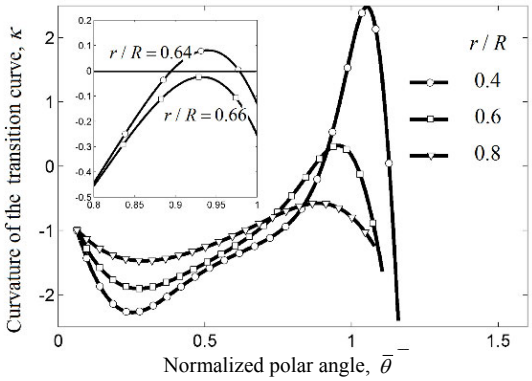

Fig. 12 Curvature as a function of normalized polar angle and size ratio r/R for a 5th-order transition curve

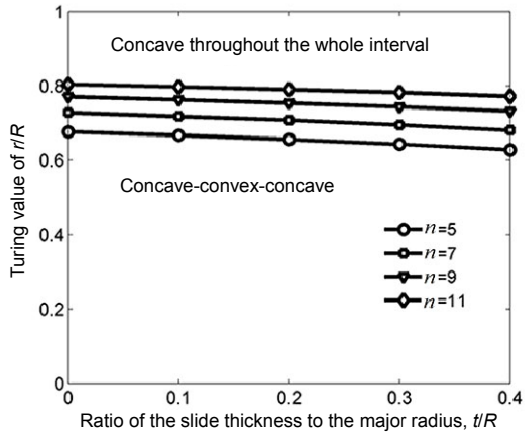

Fig. 13 Turning value of r/R as a function of t/R for different orders of transition curves

4 Discussion and conclusions

The working of the profiled chamber flow sensor requires that the transition curves must satisfy several conditions to achieve best dynamic characteristics of the transition control surface moving slide assembly. In this paper, the boundary conditions for deriving the transition curves have been given in Section 2 for the bidirectional PCF considering slide ends with more general shapes. The general polynomial expressions in polynomial forms are provided, and these can be compared with the study of Lei and Lu (2011). In Section 2, the analysis of the transition curve curvature is further work based on the study of Lei and Lu (2011). The dependence of the transition curve curvature on the size ratio of the minor radius r_2 and major radius r_1 has been analyzed. For a 5th-order polynomial function, the ratio r_2/r_1 should be larger than 0.677 to make sure the transition curve is concave through the entire range of $\theta \in [0, \pi/2]$.

Since the slides can be seen as rigid, the dynamic properties are decided by the movement of the center of mass. Therefore, the analysis work on velocity, acceleration, and jerk of polynomial functions for the transition curves in references (Lei and Lu, 2011; Lei et al., 2016) and Section 2 of this paper is applicable when considering the slide with arc-shaped ends. Further corrections are needed to eliminate the interference between the slides with the transition curves while keeping the center of mass movement properties the same as those in Section 2. The 5th-order polynomial expression is chosen as an analyzing case in the present work to analyze the interference problems. The designed transition curves considering the slides with arc ends are given in Eqs. (8)–(14) and this part of work is an important extension of the previous systematic work of Lei and Lu (2011) and Lei et al. (2016). The curvature of the transition curves considering the slides is also analyzed numerically in Section 3.2.

References

Acharyya S, Naskar TK, 2008. Fractional polynomial mod traps for optimization of jerk and Hertzian contact stress in cam surface. *Computers & Structures*, 86(3-5):322-329. https://doi.org/10.1016/j.compstruc.2007.01.045

Cai HH, Wang GJ, 2009. A new method in highway route design: joining circular arcs by a single C Bezier curve with shape parameter. *Journal of Zhejiang University-SCIENCE A*, 10(4):562-569. https://doi.org/10.1631/jzus.A0820267

Cardona A, Lens E, Nigro N, 2002. Optimal design of cams. *Multibody System Dynamics*, 7(3):285-305. https://doi.org/10.1023/A:1015278213069

Carra S, Garziera R, Pellegrini M, 2004. Synthesis of cams with negative radius follower and evaluation of the pressure angle. *Mechanism and Machine Theory*, 39(10): 1017-1032. https://doi.org/10.1016/j.mechmachtheory.2004.05.001

Chablat D, Angeles J, 2007. Strategies for the design of a Slide-o-Cam transmission. Proceedings of CK2005, International Workshop on Computational Kinematics, p.1-10.

Flocker FW, 2012. A versatile cam profile for controlling interface force in multiple-dwell cam-follower systems. *Journal of Mechanical Design*, 134(9):094501. https://doi.org/10.1115/1.4007146

Fujiki M, Ni J, Shih AJ, 2011. Tool path planning for near-dry EDM milling with lead angle on curved surfaces. *Journal of Manufacturing Science and Engineering*, 133(5): 051005. https://doi.org/10.1115/1.4004865

Hidalgo-Martínez M, Sanmiguel-Rojas E, Burgos MA, 2014. Design of cams with negative radius follower using Bezier curves. *Mechanism and Machine Theory*, 82: 87-96. https://doi.org/10.1016/j.mechmachtheory.2014.08.001

Lei H, Lu Y, 2011. Optimization of transition curve of casing cavity of profiled chamber flow sensor. *Mechanism and Machine Theory*, 46(11):1773-1783. https://doi.org/10.1016/j.mechmachtheory.2011.06.004

Lei H, Jiang GL, Jiang ZY, et al., 2010. Profiled chamber flow sensor. *Journal of Zhejiang University (Engineering Science)*, 44:1535-1539 (in Chinese).

Lei H, Hu H, Lu Y, 2016. A dynamic analysis on the transition

curve of profiled chamber metering pump. *Journal of Dynamic Systems, Measurement, and Control*, 138(7): 071003.
https://doi.org/10.1115/1.4033174

Lu Y, 2007. Profiled Chamber Flow-meter. Patent of China CN101149284 (in Chinese).

Mandal M, Naskar TK, 2009. Introduction of control points in splines for synthesis of optimized cam motion program. *Mechanism and Machine Theory*, 44(1):255-271.
https://doi.org/10.1016/j.mechmachtheory.2008.01.005

Mermelstein SP, Acar M, 2004. Optimising cam motion using piecewise polynomials. *Engineering with Computers*, 19(4):241-254.
https://doi.org/10.1007/s00366-003-0264-0

Naskar TK, Mishra R, 2012. Introduction of control points in B-splines for synthesis of ping finite optimized cam motion program. *Journal of Mechanical Science and Technology*, 26(2):489-494.
https://doi.org/10.1007/s12206-011-1004-9

Nguyen V, Kim D, 2007. Flexible cam profile synthesis method using smoothing spline curves. *Mechanism and Machine Theory*, 42(7):825-838.
https://doi.org/10.1016/j.mechmachtheory.2006.07.005

Wu L, Wu S, Yan H, 1999. Simplified graphical determination of disk-cam curvature. *Mechanism and Machine Theory*, 34(7):1023-1036.
https://doi.org/10.1016/S0094-114X(98)00088-3

Wu L, Chang W, Liu C, 2007. The design of varying-velocity translating cam mechanisms. *Mechanism and Machine Theory*, 42(3):352-364.
https://doi.org/10.1016/j.mechmachtheory.2006.03.006

Wu LM, Liu DR, Lu Y, 2009. Bilateral Profiled Chamber Flow-meter. Patent of China CN101586973 (in Chinese).

Yan HS, Cheng WT, 1999. Curvature analysis of roller-follower cam mechanisms. *Mathematical and Computer Modelling*, 29(1):69-87.
https://doi.org/10.1016/S0895-7177(98)00179-4

Yu Q, Lee HP, 1998. Influence of cam motions on the dynamic behavior of return springs. *Journal of Mechanical Design*, 120(2):305-310.
https://doi.org/10.1115/1.2826973

Appendix A Design of basic transition curve

A1 Boundary conditions

The boundary conditions and isometric condition are as follows:

$$\rho_s(0)=r_1, \tag{A1}$$

$$\rho_s(\pi/2)=r_2, \tag{A2}$$

$$\rho_s(\theta)+\rho_s\left(\frac{\pi}{2}-\theta\right)=r_1+r_2, \tag{A3}$$

$$\rho_s'(0)=\rho_s'(\pi/2)=0, \tag{A4}$$

$$\rho_s''(0)=\rho_s''(\pi/2)=0. \tag{A5}$$

A2 Derivations of the transition curve

It is assumed that $\rho_s(\theta)$ is a polynomial function with the following form:

$$\rho_s(\theta)=r_1+(r_1-r_2)\left[k_{(n+1)/2}\left(\frac{\theta}{\pi/2}\right)^{(n+1)/2}+k_{(n+1)/2+1}\left(\frac{\theta}{\pi/2}\right)^{(n+1)/2+1}+\cdots+k_n\left(\frac{\theta}{\pi/2}\right)^{n}\right], \tag{A6}$$

where $n\geq 5$ is an odd number. This expression means the condition in Eq. (A1) is satisfied. The coefficients $k_{(n+1)/2}$, $k_{(n+1)/2+1}$, …, k_n can be derived from the boundary conditions in Eq. (A2) and the 1st- and 2nd-order continuity in Eqs. (A4) and (A5) and the extended $[(n-1)/2]$th-order continuity; that is

$$\rho_s^{(n-1)/2}(0)=\rho_s^{(n-1)/2}(\pi/2)=0. \tag{A7}$$

So the Eqs. (A2) and (A4)–(A7) can be expressed by the following matrix equation:

$$\boldsymbol{K}\boldsymbol{k}=\boldsymbol{b}, \tag{A8}$$

where

$$\boldsymbol{K}=\begin{bmatrix} 1 & 1 & 1 & \cdots & 1 \\ \mathrm{A}^{1}_{\frac{n+1}{2}} & \mathrm{A}^{1}_{\frac{n+1}{2}+1} & \mathrm{A}^{1}_{\frac{n+1}{2}+2} & \cdots & \mathrm{A}^{1}_{n} \\ \mathrm{A}^{2}_{\frac{n+1}{2}} & \mathrm{A}^{2}_{\frac{n+1}{2}+1} & \mathrm{A}^{2}_{\frac{n+1}{2}+2} & \cdots & \mathrm{A}^{2}_{n} \\ \vdots & \vdots & \vdots & \vdots & \vdots \\ \mathrm{A}^{\frac{n-1}{2}}_{\frac{n+1}{2}} & \mathrm{A}^{\frac{n-1}{2}}_{\frac{n+1}{2}+1} & \mathrm{A}^{\frac{n-1}{2}}_{\frac{n+1}{2}+2} & \cdots & \mathrm{A}^{\frac{n-1}{2}}_{n} \end{bmatrix},$$

$$\boldsymbol{k}=\begin{bmatrix} k_{\frac{n+1}{2}} & k_{\frac{n+1}{2}+1} & k_{\frac{n+1}{2}+2} & \cdots & k_n \end{bmatrix}^{\mathrm{T}}, \tag{A9}$$

$$\boldsymbol{b}=\begin{bmatrix} -1 & 0 & 0 & \cdots & 0 \end{bmatrix}^{\mathrm{T}},$$

where A is the symbol for permutation. The solutions are

$$k_{\frac{n+1}{2}}=\frac{\Delta_{\frac{n+1}{2}}}{|\boldsymbol{K}|},\ k_{\frac{n+1}{2}+1}=\frac{\Delta_{\frac{n+1}{2}+1}}{|\boldsymbol{K}|},\\ k_{\frac{n+1}{2}+2}=\frac{\Delta_{\frac{n+1}{2}+2}}{|\boldsymbol{K}|},\ \cdots,\ k_n=\frac{\Delta_n}{|\boldsymbol{K}|},\tag{A10}$$

where $|\boldsymbol{K}|$ is the matrix determinant value of $\boldsymbol{K}$, Δ_i is the matrix determinant value of $\boldsymbol{K}$, in which the row i is replaced by matrix $\boldsymbol{b}$.

The isometric condition in Eq. (A3) is not directly used in derivation of the coefficients. It is interesting to find that the solution of Eq. (A8) spontaneously satisfies the isometric condition in Eq. (A3). To be rigorous, it is necessary to verify this.

Eq. (A3) indicates that

$$\rho_s\left(\frac{\pi}{2}-\theta\right)=r_2-(r_1-r_2)\left[k_{(n+1)/2}\bar{\theta}^{(n+1)/2}+k_{(n+1)/2+1}\bar{\theta}^{(n+1)/2+1}+\ldots+k_n\bar{\theta}^n\right],\tag{A11}$$

where $\bar{\theta}=\theta/(\pi/2)$, and according to Eq. (A6) we have

$$\rho_s\left(\frac{\pi}{2}-\theta\right)=r_1+(r_1-r_2)\left[k_{(n+1)/2}\left(1-\bar{\theta}\right)^{(n+1)/2}+k_{(n+1)/2+1}\left(1-\bar{\theta}\right)^{(n+1)/2+1}+\cdots+k_n\left(1-\bar{\theta}\right)^n\right].\tag{A12}$$

Comparing the coefficients of r_1 and r_2 in Eqs. (A11) and (A12) gives

$$1+k_{(n+1)/2}\bar{\theta}^{(n+1)/2}+k_{(n+1)/2+1}\bar{\theta}^{(n+1)/2+1}+\cdots+k_n\bar{\theta}^n=-k_{(n+1)/2}\left(1-\bar{\theta}\right)^{(n+1)/2}-k_{(n+1)/2+1}\left(1-\bar{\theta}\right)^{(n+1)/2+1}-\cdots-k_n\left(1-\bar{\theta}\right)^n.\tag{A13}$$

The derivation of Eq. (A13) indicates

$$\mathrm{A}^1_{\frac{n+1}{2}}k_{\frac{n+1}{2}}\bar{\theta}^{\frac{n+1}{2}-1}+\mathrm{A}^1_{\frac{n+1}{2}+1}k_{\frac{n+1}{2}+1}\bar{\theta}^{\frac{n+1}{2}}+\cdots+\mathrm{A}^1_n k_n\bar{\theta}^{n-1}=\mathrm{A}^1_{\frac{n+1}{2}}k_{\frac{n+1}{2}}\left(1-\bar{\theta}\right)^{\frac{n+1}{2}-1}+\mathrm{A}^1_{\frac{n+1}{2}+1}k_{\frac{n+1}{2}+1}\left(1-\bar{\theta}\right)^{\frac{n+1}{2}}+\cdots+\mathrm{A}^1_n k_n\left(1-\bar{\theta}\right)^{n-1}.\tag{A14}$$

Eq. (A14) means for any value of θ, the following equation stands:

$$\rho_s'(\theta)-\rho_s'\left(\frac{\pi}{2}-\theta\right)=0.\tag{A15}$$

Eq. (A15) with Eqs. (A1) and (A2) means the isometric condition in Eq. (A3) is satisfied.

Furthermore, the isometric condition in Eq. (A3) or Eq. (A15) can also prove that n should be an odd number. Supposing n is an even number, n=2m (m is any positive integer), and the transition curve function is

$$\rho_s(\theta)=r_1+(r_1-r_2)\left(k_3\bar{\theta}^3+k_4\bar{\theta}^4+\cdots+k_{2m}\bar{\theta}^{2m}\right).\tag{A16}$$

Substituting Eq. (A16) into Eq. (A15) gives

$$3k_3\left[\bar{\theta}^2-(1-\bar{\theta})^2\right]+4k_4\left[\bar{\theta}^3-(1-\bar{\theta})^3\right]+\cdots+2mk_{2m}\left[\bar{\theta}^{2m-1}-(1-\bar{\theta})^{2m-1}\right]=0,\tag{A17}$$

which should stand for any value of $\bar{\theta}$ in the range of [0, 1]. The last term of Eq. (A17) can be expanded to

$$2mk_{2m}\left[2\bar{\theta}^{2m-1}-\mathrm{C}^1_{2m-1}\frac{\pi}{2}\bar{\theta}^{2m-2}+\mathrm{C}^2_{2m-1}\left(\frac{\pi}{2}\right)^2\bar{\theta}^{2m-3}-\cdots\right],\tag{A18}$$

where C is the symbol for combination.

Thus, the term of $\bar{\theta}$ with the highest order is $4mk_{2m}\bar{\theta}^{2m-1}$. Since Eq. (A17) should stand for any value of $\bar{\theta}$, the value of k_{2m} should be 0. Therefore, the value of n cannot be an even number.

Appendix B Geometry relations in some figures and equations

B1 Geometry relations in Fig. 8 and Eq. (7)

$$OD_s=O_sD_s-O_sO<r,\\ O_sD_s=R,\\ O_sO=R\cos\theta_1-r\cos\theta_2,\\ r_2=R-(R\cos\theta_1-r\cos\theta_2)<r.$$

B2 Geometry relations in Fig. 9 and Eq. (9)

Fig. B1 shows the geometry relations of a slide.

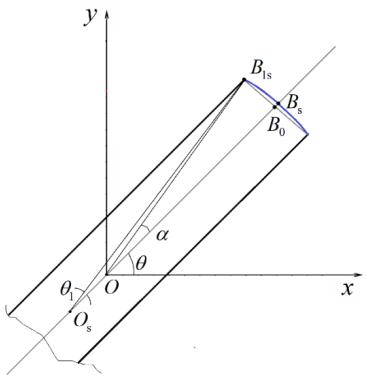

Fig. B1 Geometry relations of a slide

$$\tan\alpha=\frac{t/2}{OB_0},$$

$$OB_0=OB_s-B_0B_s,$$

$$OB_s=\rho_s,$$

$$B_0B_s=O_sB_s-O_sB_0,$$

$$O_sB_s=R,$$

$$O_sB_0=R\cos\theta_1,$$

$$\alpha(\theta)=\arctan\frac{t/2}{\rho_s(\theta)-R(1-\cos\theta_1)}.$$

中文概要

题　目： 考虑转子为圆弧顶的流量传感器异型腔过渡曲线的优化设计

目　的： 为了使作者设计的一种新型异型腔流量传感器获得更好的密封性能和转子动态特性，本文重点研究转子为圆弧顶时的流量传感器定子型腔过渡曲线的优化设计。

创新点： 将转子顶端设计为圆弧形状，优化了转子与定子内腔之间的密封性能，但增加了曲线设计的难度。本文给出了设计方法和相关的公式推导，并提出过渡曲线的设计需要考虑曲线凸凹形状这个因素。

方　法： 1. 提出“基本过渡曲线”的概念并总结多项式函数描述的过渡曲线的优化设计方法，给出边界条件和求解方法；2. 分析过渡曲线的凸凹形状对设计加工的影响；3. 分析圆弧顶转子与定子内腔可能产生的干涉问题，给出考虑转子顶端为圆弧形状时的过渡曲线的设计方法，并分析不同阶数的多项式函数所描述的过渡曲线的凸凹形状特点。

结　论： 1. 本文设计的过渡曲线可以使流量传感器的转子与定子内腔获得更好的密封性能，且转子的动态特性达到最优；2. 考虑过渡曲线的凸凹形状可降低加工工艺的难度。

关键词： 转子流量传感器；过渡曲线；转子动态特性